Lift maximization with uncertainties for the optimization of high-lift devices

Z. Tang[1,2], J. Périaux[2], G. Bugeda[2,*,†] and E. Oñate[2]

[1]*College of Aerospace Engineering*, *Nanjing University of Aeronautics and Astronautics*, *Nanjing*, *China*
[2]*Centre Internacional de Métodes Numérics en Enginyeria*, *Departament Resistència de Materials i Estructures a l'Enginyeria*, *Universitat Politécnica Catalunya*, *C/Gran Capitán s/n*, *Campus Nord UPC*, *Módulo C1*, *08034 Barcelona*, *Spain*

SUMMARY

In this paper, the aerodynamic shape optimization problems with uncertain operating conditions have been addressed. After a review of robust control theory and the possible approaches to take into account uncertainties, the use of Taguchi robust design methods in order to overcome single point design problems in aerodynamics is proposed. Under the Taguchi concept, a design with uncertainties is converted into an optimization problem with two objectives which are the mean performance and its variance, so that the solutions are as less sensitive to the uncertainty of the input parameters as possible. Furthermore, the modified non-dominated sorting genetic algorithms are used to capture a set of compromised solutions (Pareto front) between these two objectives. The flow field is analyzed by Navier–Stokes computation using an unstructured mesh. In order to reduce the number of expensive evaluations of the fitness function a response surface modeling is employed to estimate the fitness value using the polynomial approximation model. During the solution of the optimization problem, a semi-torsional spring analogy is used for the adaption of the computational mesh to all the obtained geometrical configurations. The proposed approach is applied to the robust optimization of the 2D high-lift devices of a business aircraft by maximizing the mean and minimizing the variance of the lift coefficients with uncertain free-stream angle of attack at landing flight condition. Copyright © 2009 John Wiley & Sons, Ltd.

---

*Correspondence to: G. Bugeda, Centre Internacional de Métodes Numérics en Enginyeria, Departament Resistència de Materials i Estructures a l'Enginyeria, Universitat Politécnica de Catalunya, C/Gran Capitán s/n, Campus Nord UPC, Módulo C1, 08034 Barcelona, Spain.
†E-mail: bugeda@cimne.upc.edu

1. INTRODUCTION

In spite of the important effect of operating and manufacturing uncertainties on the performance, traditional aerodynamic shape optimization has focused on obtaining the best design given a set of deterministic flow conditions. Clearly, it is important to maintain near-optimal performance levels at off-design operating conditions, and to ensure that performance does not degrade appreciably when the component shape differs from the optimal one due to manufacturing tolerances and normal wear and tear. These requirements naturally lead to the idea of robust optimal design wherein the concept of robustness in front of different perturbations is built into the design optimization procedure.

The recognition of the importance of incorporating the probabilistic nature of the variables involved in designing and operating complex systems has led to several investigations in the recent past. Some of the basic principles of robust optimal design are discussed by Egorov *et al.* [1]. They make the observations that (a) robust design optimization is in essence multi-objective design optimization because of the presence of the additional objective (robustness) and (b) the addition of the robustness criterion may result in an optimal solution that is substantially different from that obtained without this criterion. Different approaches to robust optimal design are also mentioned in this paper.

The main objective of this paper is to develop a robust aerodynamic optimization scheme for achieving consistent improvements of the performance over a given range of uncertainty parameters. This scheme has the following two major advantages: (a) it prevents severe degradation in the off-design performance and (b) it is not sensitive to the number of design points.

The imposition of the additional requirement of robustness results in a multiple-objective optimization problem requiring appropriate solution procedures. Typically, the costs associated with multiple-objective optimization are relevant. Therefore, efficient multiple-objective optimization procedures are crucial for the rapid deployment of the principles of robust design in industry. Here, we focus on the applications of an evolutionary algorithm for multiple-objective optimization [2] by using Pareto front concept. Applications of this evolutionary method to some difficult model problems involving the complexities (convex, non-convex, discrete or discontinuous Pareto front) are also presented in Reference [2]. The computed Pareto-optimal solutions closely approximate the global Pareto front and exhibit good solution diversity. Many of these solutions were obtained with relatively small population sizes.

The final goal of this study is to propose an algorithm to take into account the uncertainties related with fluctuating operating conditions integrating them into an automatic shape optimization problem in aerodynamics. We propose to use Taguchi robust design methods in order to overcome single point design problems. The latter techniques produce solutions that perform well for the selected design point but have poor off-design performance. Under the Taguchi concept, a design with uncertainties is converted into an optimization problem with two objectives that are mean performance and its variance, so that the solutions are as less insensitive to the uncertainty of the input parameters as possible. Furthermore, the multi-criterion evolutionary algorithms are used to capture a set of compromised solutions (Pareto front) between these two objectives. The flow field is analyzed by Navier–Stokes (N-S) computation. In order to reduce the number of expensive evaluations of fitness function, response surface modeling (RSM) is employed to estimate fitness value using the approximate model. During the solution of the optimization problem a Semi-torsional Spring Analogy is used to adapt a single computational mesh to all geometrical configurations obtained during the optimization process. The proposed approach is applied to the

robust optimization of the 2D high-lift devices of a business aircraft, by maximizing the mean and minimizing the variance of the lift coefficients under uncertain free-stream angle of attack at landing flight condition.

2. ROBUST CONTROL AND TAGUCHI METHODOLOGY

Many products are now routinely designed with the aid of computer models. Given the inputs designable engineering parameters and the parameters representing manufacturing process conditions the model generates the product's quality characteristics. The quality improvement problem is to choose the designable engineering parameters such that the quality characteristics are uniformly good in the presence of variability of different conditions.

We consider objective functions of the form $f : X \otimes B \longrightarrow \Re$, where $x \in X$ represents decision variables, inputs (designs) controlled by the engineer, $b \in B$ represents uncertainty, inputs not controlled by the engineer and $f(x, b)$ quantifies the loss suffered by design x under the uncertain conditions b.

Our (unattainable) goal is to find $x^* \in X$ such that, for every $b \in B$,

$$f(x^*, b) \leqslant f(x, b) \quad \forall x \in X \tag{1}$$

The unsolvable problem of finding $x^* \in X$ that simultaneously minimizes $f(x, b)$ for each $b \in B$ is the central problem of statistical decision theory: and a decision rule that simultaneously minimizes risk for every possible state of nature. A standard way (e.g. Ferguson [3]) of negotiating this problem is to replace each $f(x, \cdot)$ with a real-valued attribute of it, e.g.

Minimax principle:

$$\min_{x \in X} \phi(x) \quad \text{where } \phi(x) = \sup_{b \in B} f(x; b) \tag{2}$$

Bayes principle:

$$\min_{x \in X} \phi(x) \quad \text{where } \phi(x) = \int_B f(x, b) p(b) \, \mathrm{d}b \tag{3}$$

where p denotes a probability density function (PDF) on B.

The *minimax* principle is extremely conservative. It seeks to protect the decision-maker against the worst-case scenario. The Bayes principle seeks to minimize average loss in a way that can be customized (via the choice of p) to the application. This formulation of the quality control problem was first proposed by Welch *et al.* [4], although their suggestion appears to have had little effect on engineering practice.

Although the above formulation and proposed solution of the quality improvement problem is modern, the problem itself predates the engineering community's use of computer models. To motivate our own approach to this problem, and the more general robust design problem, we briefly summarize the contributions of Taguchi. See Roy [5] for a broader context and a more detailed discussion of Taguchi's far-ranging contributions to quality engineering.

In the statistical approach, one considers the fluctuating operating conditions $\mathbf{b} = (b_i)_{i=1,\dots,N}$ as samples of random variables $\mathbf{B} = (B_i)_{i=1,\dots,N}$, whose statistical characteristics are known (mean $\boldsymbol{\mu}_\mathbf{B} = (\mu_B^i)_{i=1,\dots,N}$, variance $\boldsymbol{\sigma}_\mathbf{B}^2 = (\sigma_B^{2\,i})_{i=1,\dots,N}$, etc.). One also suppose, for the sake of simplicity,

that the random variables $(B_i)_{i=1,...,N}$ are independent. The statistical characteristics of operating conditions can be determined by experimental measurements or engineering experience. Gaussian PDFs or truncated Gaussian PDFs are often used in practice (see [6] for instance).

The main consequence of this assumption is that the cost function of the problem is also a random variable f. According to the Von Neumann–Morgenstern decision theory, the best choice is then to select the design that leads to the best expected fitness. This is known as the maximum expected values (MEV) criterion. The decision or design that minimizes the risk is known as the *Bayes' decision* and is solution of the following problem:

$$\text{Minimize } \mu_f = \int_{\Omega(B)} f(x,b)\rho_B(b)\,db, \quad x \in \Re^n \tag{4}$$

$\Omega(B)$ and ρ_B are the range and the PDF of the random variable B. Then, the MEV criterion just consists in minimizing the statistical mean μ_f of the cost function.

This approach is a significant improvement over previous methods. The robust design problem is now considered with a rigorous statistical framework. This allows to take into account not only the random fluctuations of the fitness in the optimization problem but also to take care about the frequency of the occurrence of the events, thanks to PDFs. Then, the most probable events have a larger influence in the decision than extreme and unlikely events.

However, problem (4) does not address the variability of the fitness. The mean value of the fitness is the only criterion that is considered in the *Bayes' decision*. For engineering problems, one also would like to select a design for which the fitness is not subjected to large variations when operating conditions fluctuate. Then, a second criterion is often joined to the MEV criterion that relies on the minimization of the variance σ_f^2 of the fitness:

$$\text{Minimize } \begin{cases} \mu_f = \displaystyle\int_{\Omega(B)} f(x,b)\rho_B(b)\,db, \\[2mm] \sigma_f^2 = \displaystyle\int_{\Omega(B)} (f(x,b)-\mu_f)^2\rho_B(b)\,db, \end{cases} \quad X \in \Re^n \tag{5}$$

This approach aims at determining a tradeoff between the expected fitness and the expected fitness variation as operating conditions randomly fluctuate. Although this approach is satisfactory from theoretical and practical viewpoints, its application is not straightforward. Particularly, the estimation of the mean and variance can be tedious for complex CFD applications. This issue is detailed below.

To estimate the mean and variance of the random variable f, one can simply use statistical estimators in a classical Monte-Carlo approach. A sample of operating conditions $(b_i)_{i=1,...,N}$ if size N is generated according to the PDF ρ_B. Then, unbiased estimators of the mean and variance are:

$$\begin{aligned} \mathbf{M}_f &= \frac{1}{N}\sum_{i=1}^{N} f(x,b_i) \\[2mm] S_f^2 &= \frac{1}{N-1}\sum_{i=1}^{N}(f(x,b_i)-\mathbf{M}_f)^2 \end{aligned} \tag{6}$$

This approach does not suffer from *point-optimization effect* since the sample $(b_i)_{i=1,...,N}$ is generated randomly according to the PDF ρ_B.

This approach drives to the solution of a multi-objective optimization problem. The test cases presented in this work have been solved using a modification of a non-dominated sorting genetic algorithm (NSGA) [7].

There exist several variants of GAs for multi-objective optimization problems; see, for example, vector evaluated GAs (VEGAs) [8] and NSGAs [9]. For further information on GAs for multi-objective optimization see References [10–14] and references therein.

3. 2D N-S SOLVER ON UNSTRUCTURED MESH

In the examples shown at the end of this paper we have solved the 2D N-S equations by using a finite volume Galerkin method on unstructured meshes. A 2D unstructured mesh has been generated by the pre/post-processing software **GID** of CIMNE. To solve the Euler part of the equations, a Roe scheme has been used. To compute turbulent flows a k–ε model has been chosen. Near-wall turbulence has been computed by a two-layer approach. Time-dependant problems have been solved using a fourth-order Runge–Kutta scheme.

4. ADAPTIVE RESPONSE SURFACE MODELING (ARSM) METHODS

One of the most important advantages obtained by using RSMs [15] in optimization is a significant reduction in the computational cost. This allows the user to perform global optimization and reliability-based optimization, which are otherwise prohibitively computationally expensive. In addition, the use of response surface models allows the design engineer to quickly perform a variety of tradeoff studies that provide information about the sensitivity of the optimal aircraft design with respect to changes in performance criteria and to off-design conditions.

The reduction in the computational cost of optimization provided by response surface models motivates their use in the modeling of data, despite the fact that, under certain conditions, they can produce some numerical noise.

4.1. RSM methods

In many RSM applications, either linear or quadratic polynomials are assumed to accurately model the observed response values. If n_s analysis are performed and $p=1,\ldots,n_s$, then a quadratic response surface (RS) model has the form

$$y^{(p)} = c_0 + \sum_{1 \leqslant j \leqslant n_v} c_j x_j^{(p)} + \sum_{1 \leqslant j \leqslant k \leqslant n_v} c_{(n_v-1+j+k)} x_j^{(p)} x_k^{(p)} \tag{7}$$

where $y^{(p)}$ is the response; $x_j^{(p)}$ and $x_k^{(p)}$ are the n_v design variables; and c_0, c_j, and $c_{(n_v-1+j+k)}$ are the unknown polynomial coefficients. Note that there are $n_t = (n_v+1)(n_v+2)/2$ coefficients (i.e. model terms) in the quadratic polynomial. This polynomial model may be written in matrix notation as

$$y^{(p)} = C^{\mathrm{T}} \bar{X}^{(p)} \tag{8}$$

where C is the vector of length n_t of unknown coefficients to be estimated,

$$C = [c_0, c_1, \ldots, c_{n_t-1}] \tag{9}$$

and $\bar{X}^{(}p)$ is the vector of length n_t corresponding to the form of the $x_j^{(p)}$ and $x_k^{(p)}$ terms in the polynomial model (7). For the pth observation this is

$$\bar{X}^{(p)} = [1, x_1^{(p)}, x_2^{(p)}, \ldots, x_{n_v}^{(p)}, (x_1^{(p)})^2, x_1^{(p)} x_2^{(p)}, \ldots, (x_{n_v}^{(p)})^2] \tag{10}$$

Note that there is a difference between the pth vector of independent variables, $X^{(p)}$, and the pth vector of independent variables mapped into the form of the polynomial model, $\bar{X}^{(p)}$.

Estimating the unknown coefficients requires n_s analysis, where $n_s \geqslant n_t$. Under such conditions, the estimation problem may be formulated in matrix notation as

$$Y \approx XC \tag{11}$$

where Y is the vector of n_s observed response values,

$$Y = [y^{(1)}, y^{(2)}, \ldots, y^{(n_s)}] \tag{12}$$

and X is the matrix formed by the n_s row vectors $\bar{X}^{(p)}$ which is assumed to have rank n_t. Thus, X may be expressed as

$$X = \begin{bmatrix} 1 & x_1^{(1)} & x_2^{(1)} & \ldots & (x_{n_v}^{(1)})^2 \\ \vdots & \vdots & \vdots & \ddots & \vdots \\ 1 & x_1^{(n_s)} & x_2^{(n_s)} & \ldots & (x_{n_v}^{(n_s)})^2 \end{bmatrix} \tag{13}$$

The unique least-squares solution to Equation (11) is

$$\hat{C} = (X^{\mathrm{T}} X)^{-1} X^{\mathrm{T}} Y \tag{14}$$

where $(X^{\mathrm{T}} X)^{-1}$ exists if the rows of X are linearly independent. When C is substituted by $\hat{C}$ into Equation (8), values of the response may be predicted at any location $\mathbf{x}$ by mapping $\mathbf{x}$ into $\bar{X}^{(p)}$. In matrix notation this corresponds to

$$\hat{Y} = \hat{C}^{\mathrm{T}} \bar{X}^{(p)} \tag{15}$$

Note that if $n_s > n_t$ the system of equations is overdetermined. Thus, the predicted response values (from the polynomial model) at the original sample locations may differ from the observed response values at the sampled locations.

Polynomial RS models can be considered as *global* models in which all of the n_s observed values of the response are equally weighted in the fitting of the polynomial surface. At an unsampled location in design space, $\mathbf{x}$, response observations that are near to $\mathbf{x}$ (in the sense of Euclidean distance) have an equal influence on the predicted response, $\hat{f}(\mathbf{x})$, as the response observations that are far from $\mathbf{x}$. It can be argued that such a global model may not be the best approximation if the true unknown response has many real local optima (as opposed to the artificial local optima created by numerical noise). In such a situation an approximation scheme having *local* modeling properties may be more attractive, i.e. adaptive response methods (ARSM).

4.2. ARSM methods

Given design variables, objectives, and the initial design space, experimental designs (points in the design space) are generated according to a formal planning strategy, e.g. central composite designs. Values of the objective function are evaluated through the computation intensive analysis and simulation processes. The quadratic response surface model, or surrogate, is fitted to the data using the usual least-square method. In the ARSM, a global optimization algorithm, GAs, is used to find the global optimum. Following this step, the value of the actual objective function at the optimum of the surrogate is calculated through an evaluation of the computation-intensive objective function. If the value of the actual objective function at the surrogate optimum is better than the values at all other experimental designs, the point is added to the set of experimental designs for the following iteration because the point represents a promising search direction. All experimental designs and the accepted model optimum are recorded in a design library. After each design iteration, a threshold, or cutting plane, is used to reduce the design space. In this algorithm, the second highest value of the objective function in the set of experimental designs is chosen as the threshold. If this second highest value cannot help to reduce the design space, the next highest value of the design function will be used, and so on.

5. SEMI-TORSIONAL SPRING ANALOGY FOR MESH MOVEMENT

During any shape optimization process there is a need for a simple, robust, and computationally efficient scheme for maintaining element quality during mesh deformation. This can be provided by a spring analogy approach. This scheme must work in both 2D and 3D, be able to handle large deformations, and work well for fully unstructured meshes. Paper [16] presented such a scheme, developed as an extension of the 2D semi-torsional approach. We have used it in our optimization approach to perform 2D multi-element unstructured mesh movement due to slat/flap position modifications. This has allowed to use the same computational mesh for all the different computational geometries obtained during the solution of the optimization problem.

5.1. Lineal spring analogy

Spring analogy models consist in considering the mesh as an assembly of springs with a given stiffness for each one. Each of the edges of the mesh is considered as a spring. Then, after the modification of the geometry of the boundary, the new resulting mesh is obtained as the new equilibrated position of the springs network.

The lineal spring stiffness k_{ij} for a given element edge $i-j$ takes the following general form:

$$k_{ij}^n = \frac{\lambda}{[(y_{1,i}^n - y_{1,j}^n)^2 + (y_{2,i}^n - y_{2,j}^n)^2 + (y_{3,i}^n - y_{3,j}^n)^2]^\beta} \qquad (16)$$

where the superscript n denotes time step, $(y_{1,i}^n, y_{2,i}^n, y_{3,i}^n)$ and $(y_{1,j}^n, y_{2,j}^n, y_{3,j}^n)$ are the spatial coordinates of the two nodes connected by the edge $i-j$ at time step n, and λ and β are coefficients. The fictitious spring force $\mathbf{F}_{ij}^n$ acting on node i from edge $i-j$ is

$$\mathbf{F}_{ij}^n = k_{ij}^n (\boldsymbol{\delta}_j^n - \boldsymbol{\delta}_i^n) \qquad (17)$$

where $\boldsymbol{\delta}_j^n$ and $\boldsymbol{\delta}_i^n$ are nodal displacements of node j and i at step n, respectively.

The static equilibrium equation for node i at time step n is

$$\sum_{j=1}^{NE_i} k_{ij}^n (\boldsymbol{\delta}_j^n - \boldsymbol{\delta}_i^n) = 0 \tag{18}$$

where N_{ei} is the number of nodes directly connected to node i through fictitious springs. A system of equations is derived by applying the equilibrium equation to all nodes in the mesh.

Nodal coordinates are updated by adding the nodal displacements to the old coordinates:

$$\mathbf{y}_i^n = \mathbf{y}_i^{n-1} + \boldsymbol{\delta}_i^n \tag{19}$$

The coefficient β is often taken to be 0.5, which means that the stiffness is inversely proportional to the length of the edge, and $\lambda = 1$.

5.2. Semi-torsional spring analogy

A semi-torsional spring analogy model is similar to the lineal formulation, with angle information incorporated into the spring stiffness. Neither displacement formulation nor force transformation is needed, and this approach is therefore easy to implement [16]. For 2D triangular elements, a semi-torsional stiffness of an edge $i - j$ was proposed by Blom [17]

$$k_{ij}^{\text{semi-torsional}} = \frac{k_{ij}^{\text{lineal}}}{\theta} \tag{20}$$

where θ is the angle facing the edge on an element. However, this semi-torsional model is not directly applicable to 3D elements. Moreover, an internal edge in a 2D triangular mesh is attached to two elements, and faces two angles that are usually different in magnitude. The above definition gives different stiffness values to a single edge when it is considered on each of its two attached elements.

To deform 2D/3D unstructured meshes for solving moving boundary problems, we propose a semi-torsional spring analogy model based on Zeng's previous work [16], in which the stiffness of an edge is defined as the sum of its linear stiffness and its semi-torsional stiffness, with the semi-torsional stiffness depending on the angle facing the edge, i.e.

$$\begin{aligned} k_{ij} &= k_{ij}^{\text{lineal}} + k_{ij}^{\text{semi-torsional}} \\ k_{ij}^{\text{semi-torsional}} &= k \sum_{m=1}^{NE_{ij}} \frac{1}{\sin^2 \theta_m^{ij}} \end{aligned} \tag{21}$$

where the lineal stiffness is defined as in Equation (16), NE_{ij} is the number of elements sharing edge $i - j$, and θ_m^{ij} is the facing angle, defined as the angle that faces the edge $i - j$ on the mth element attached to the edge. k is a coefficient having the dimension of the stiffness. In all our numerical experiments, we set the value of the coefficient to be 1.0. On a tetrahedron with vertices i, j, k, and l, the angle that faces the edge $i - j$ is taken as the angle formed between triangle Δ^{ikl} and triangle Δ^{jkl}.

By substituting (21) into (17), the spring forces on nodes i and j are expressed as

$$[F_{ij}] = \left(\frac{\lambda}{l_{ij}} + k \sum_{m=1}^{NE_{ij}} \frac{1}{\sin^2 \theta_m^{ij}} \right) [B][u_{ij}] \tag{22}$$

where $[F_{ij}]=[F_{ix}, F_{iy}, F_{iz}, F_{jx}, F_{jy}, F_{jz}]^{\mathrm{T}}$, $[u_{ij}]=[u_i, v_i, w_i, u_j, v_j, w_j]^{\mathrm{T}}$ are vectors of spring forces and displacements at nodes i and j, $[B]$ is a 6×6 matrix whose elements are given by $B_{pq}=-\delta_{pq}+\delta_{p,q+3}+\delta_{p+3,q}$, with $\delta_{pq}=1$ if $p=q$ and $\delta_{pq}=0$ if $p\neq q$.

For a 2D triangular mesh one edge within the mesh shares two elements and Equation (21) simplifies to

$$k_{ij}^{\text{semi-torsional}}=k\left(\frac{1}{\sin^2\theta_1}+\frac{1}{\sin^2\theta_2}\right) \tag{23}$$

where θ_1 is the angle facing edge $i-j$ on the triangle Δ_{ijl}, θ_2 is the angle facing edge $i-j$ on Δ_{ijk}, and k, l, i, and j are the vertices of the elements.

In a 2D triangular mesh, spring forces on the edge $i-j$ are

$$[F_{ij}]=\left(\frac{\lambda}{l_{ij}}+k\left(\frac{1}{\sin^2\theta_1}+\frac{1}{\sin^2\theta_2}\right)\right)[B^*][u_{ij}] \tag{24}$$

where $[F_{ij}]=[F_{ix}, F_{iy}, F_{jx}, F_{jy}]^{\mathrm{T}}$, $[u_{ij}]=[u_i, v_i, u_j, v_j]^{\mathrm{T}}$, and $[B^*]$ is a 4×4 matrix whose elements are given by $B_{pq}^*=-\delta_{pq}+\delta_{p,q+2}+\delta_{p+2,q}$.

With the above definition for semi-torsional stiffness, an angle approaching 0 or π makes the edge facing this angle very stiff, which prevents further change in the angle and thus avoids element inversion.

5.3. Boundary improvement

Since the static equilibrium equations for the mesh are elliptic, the principle of Saint Venant holds for deformation of the mesh. Therefore, boundary displacement does not spread far into the mesh. A boundary-improvement technique was suggested to handle this localization of deformation [18]. The stiffness of springs adjacent to the boundary was increased so that surface displacement could be spread further into the mesh. To implement this, the coefficient λ is magnified by a constant factor for springs adjacent to the boundary.

Several layers of elements near the boundary can be made stiffer by this boundary improvement technique. In our experiments, we imposed one layer of boundary stiffness modification by increasing λ from 1.0 to 3.5.

Some additional techniques to improve this situation can be seen in [19].

5.4. Mesh testing results

We have implemented the semi-torsional model for 2D multi element airfoil geometries with slat and flap movement, see Figure 1. In this example, the main body of an airfoil is fixed and the position and the orientation of slat and flap are modified. Then, the interior mesh is modified by using above analogy methods according to the boundary displacement. Figure 1 shows the mesh movement provided for different positions of slat and flat.

6. APPLICATION TO HIGH-LIFT DEVICE OPTIMIZATION

In order to test the proposed approach the robust optimization of a high-lift device has been faced. The goal of the optimization is to maximize C_l at landing fly condition by modifying the positions and orientations of slat and flap. The aerodynamic coefficients are computed using N-S flow solver.
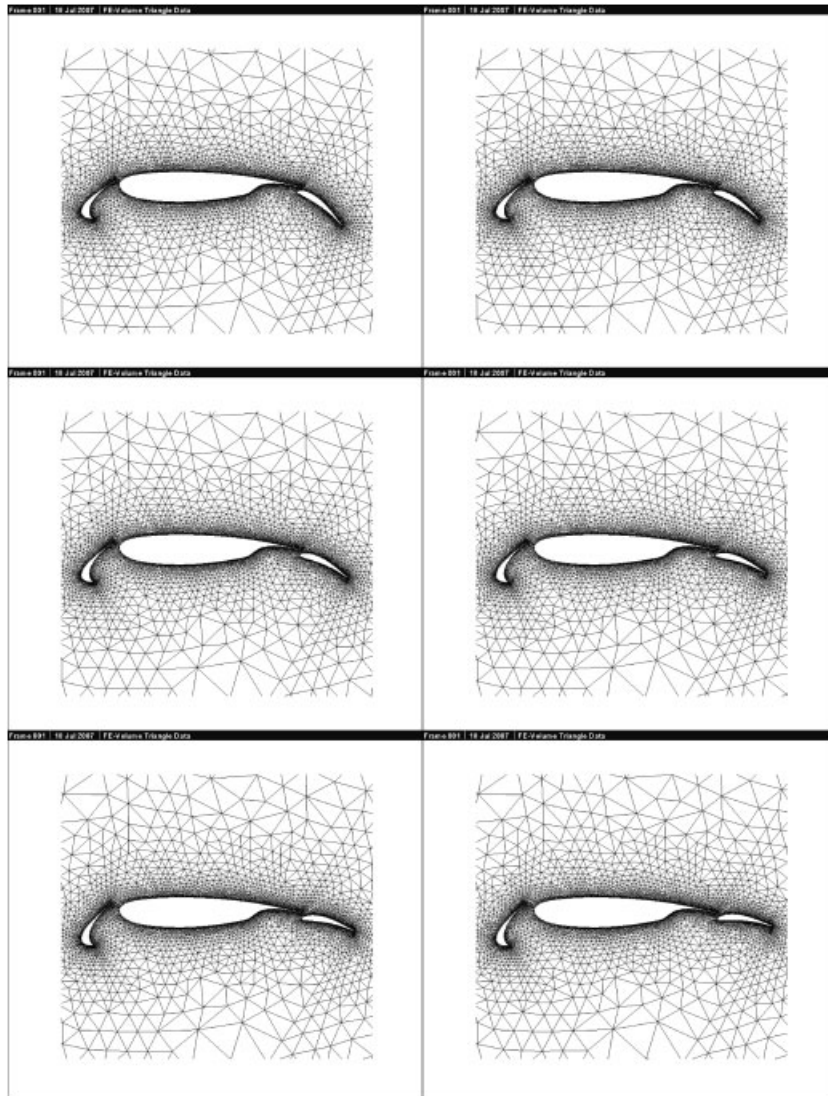
Figure 1. Example of 2D springs methods for unstructured mesh movement. Mesh movement provided for different positions of slat and flat.

Here the design variables are the positions (2 coordinates for each one) and angles of slat and flap, so that we have six design variables in total.

6.1. Single-point lift maximization at landing flight condition

For landing configurations, we only concern about the maximum lift, because in this situation drag is considered as convenient. So that the optimization problem is defined as
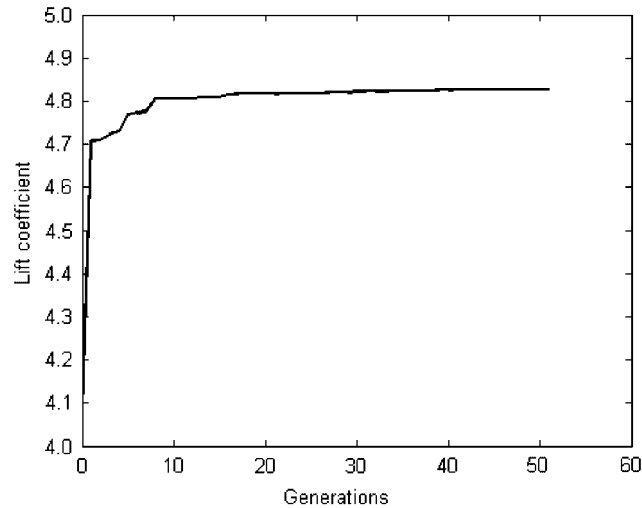
$$\max C_l \tag{25}$$
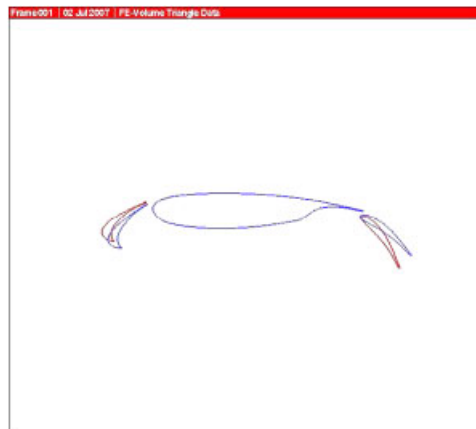
Figure 2. Convergence history of lift coefficient.

Figure 3. Optimized multielement airfoil configuration for landing. Optimized flap located below the original position. Optimized slat located on top of the original position.

The nominal operating condition is defined for landing conditions by the free-stream incidence $\alpha = 15°$, Mach number $M_\infty = 0.15$, and Reynolds number $Re = 1.8 \times 10^6$.

Figure 2 shows the convergence history of lift coefficient obtained during the optimization process. The optimized airfoil slat and flap positions are shown in Figure 3 compared with the baseline multi element airfoil. The optimized flap is located below the original position whereas the optimized slat is located on top of the original position. The optimized pressure distribution is shown in Figure 4. Table I gives the detailed evolution of the lift coefficient value during the optimization process.
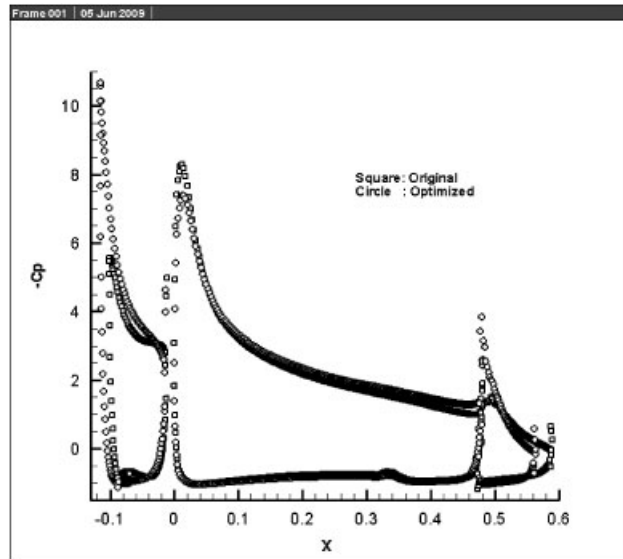
Figure 4. Comparison of pressure distributions between optimized and baseline for landing.

Table I. Lift coefficient values during optimization.

Generations	0	10	20	30	40	50
C_l	4073	4805	4816	4822	4825	4827

6.2. Lift maximization with uncertain angle of attack at landing flight condition

In this case we assume that the free-stream angle of attack is subject to random fluctuations. For simplicity, we assume that its PDF is uniform in the interval $[15-2^\circ, 15+2^\circ]$. The mean angle of attack corresponds to the nominal incidence 15°. Free-stream Mach number is $M_\infty = 0.15$ and Reynolds number $Re = 1.8 \times 10^6$.

Uncertainties in the free-stream Mach number and the Reynolds number could also be taken into account. Nevertheless, there is very few information available about the values and statistical distributions of this uncertainties that can be considered for realistic cases. The NODESIM project (see [20]) has developed different actions in order to obtain this type of information.

The mathematical formulation of the resulting optimization problem is defined as

$$\max C_l \quad \text{at } M_\infty = 0.15, \quad \alpha = [15-2^\circ, 15+2^\circ] \tag{26}$$

According to the Taguchi robust control theory, the above design problem with uncertainties can be converted into the following two-objective optimization problem, one objective is the mean value
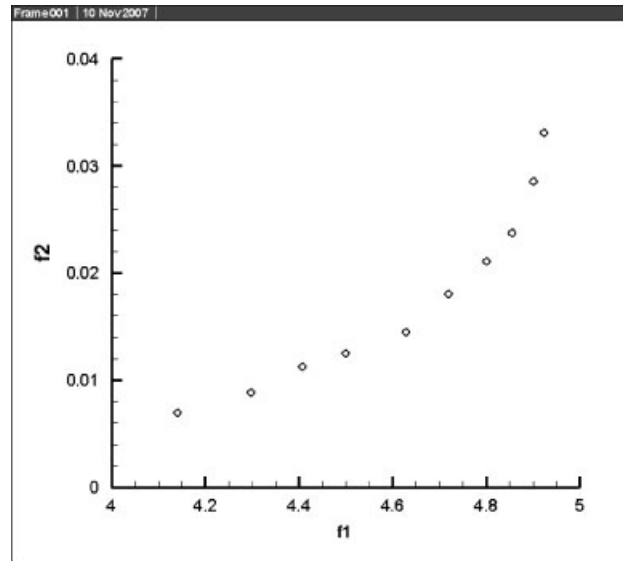
Figure 5. Pareto front between mean lift and its variance.

of the lift coefficient, and the other is the variance of lift coefficient over the range of uncertainty

$$\max f_1 = \mu_{C_l} = \frac{1}{N} \sum_{i=1}^{N} C_{li}$$
$$\min f_2 = \sigma_{C_l} = \frac{1}{N-1} \sum_{i=1}^{N} (C_{li} - \mu_{C_l})^2$$

(27)

where $N=5$, $M_\infty=0.15$, and $\alpha_i = [13, 14, 15, 16, 17°]$.

The above two-objective optimization problem drives to the solution of a multi-objective optimization problem. There exist several variants of GAs for multi-objective optimization problems; see for example VEGAs [8] and NSGAs [9]. For further information on GAs for multi-objective optimization, see References [10, 11] and references therein.

The test case presented in this work has been solved using a modification of an NSGA. More recent algorithm such as SPEA2 [11], epsilon-MOEA [21], or NSGA-II [22] (the improvement of NSGA) could also have been chosen. Nevertheless, the main objective of this work is the integration of different tools for the solution of robust design problems. Obviously, any improvement in any of the integrated tools should produce a global improvement of the whole process.

Figure 5 shows the compromised Pareto front of the above two-objective optimization problem. Figure 6 illustrates the optimized airfoil slat and flap positions of one solution on Pareto front (with $f_1 = 4.72$) compared with the baseline and traditional one-point optimized shape. The robust optimized flap position is located below the original and the traditional designed (Section 6.1) positions, whereas the robust optimized slat position is located between the original and the traditional designed (Section 6.1) positions. Streamlines over optimized airfoil are shown in Figure 7. Two clear vortices appear behind the slat and the flap. The optimized pressure distribution is shown in Figure 8.
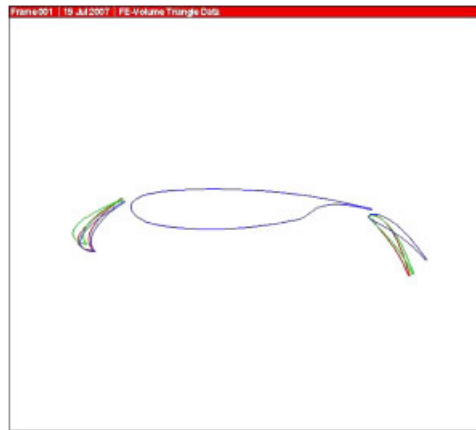
Figure 6. Robust optimized multi element airfoil configuration for Landing with $f_1 = 4.72$. Robust optimized flap located below the original and the traditional designed positions. Robust optimized slat located between the original and the traditional designed positions.
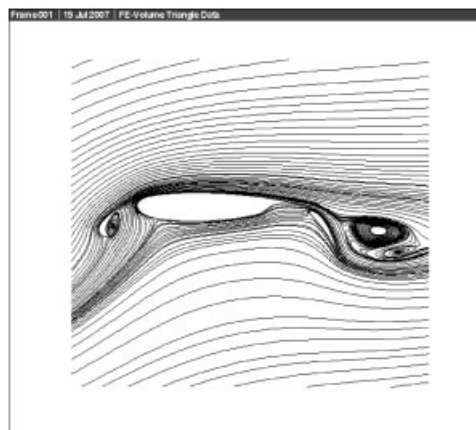

Figure 7. Stream lines over the robust optimized airfoil obtained with $f_1 = 4.72$.

Figure 9 shows a comparison between different robust optimized designs corresponding to $f_1 = 4.62$, 4.72, 4.78, and 4.83, the traditional single-point optimized design, and the baseline airfoil. We can see how the lift coefficient of the robust optimized airfoils are not as sensitive to the fluctuation of the angle of attack as the single-point optimized one. This is also illustrated by the value of C_l for the optimized and baseline airfoils in Table II. Nevertheless, the cost to be paid for this behavior is that the lift coefficient of the robust design is generally below than the single-point optimized one. On the other side, it is possible to obtain designs with mean values of lift coefficient even higher than the single-point optimized one, like the points placed more to the right in Figure 7, but then its behavior is, in fact, more sensitive with respect to the angle of attack. In these last cases, the value of C_l for $M_\infty = 0.15$ is not higher than for the single-case
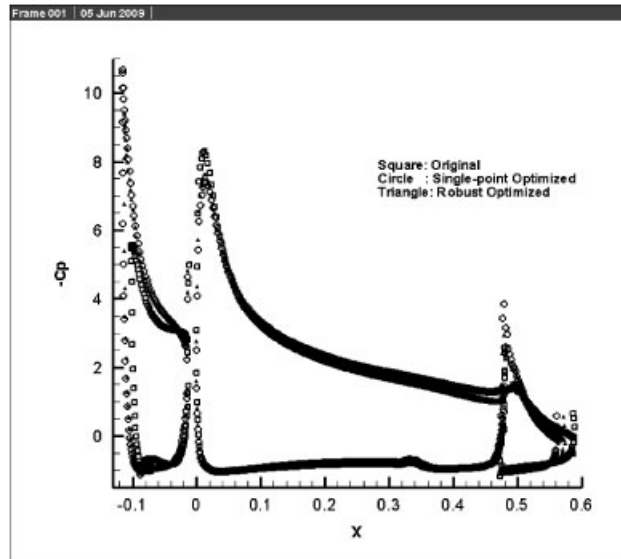
Figure 8. Comparison of pressure distributions between baseline, robust optimized with $f_1 = 4.72$, and baseline airfoils for landing.
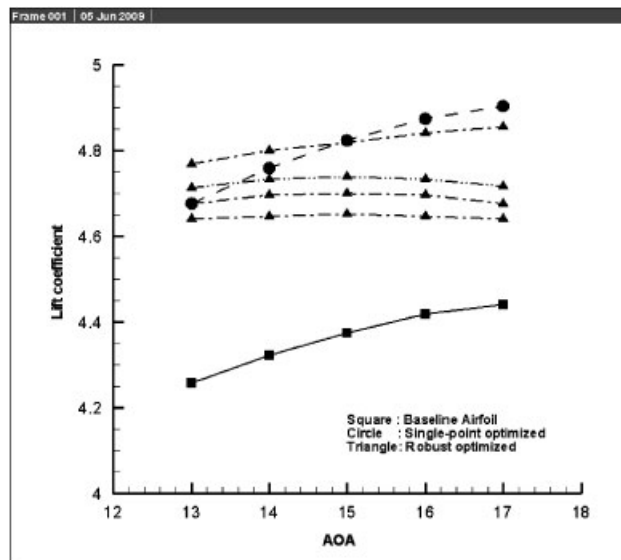

Figure 9. Comparison of the lift coefficient between different robust optimized designs corresponding to $f_1 = 4.62$, 4.72, 4.78, and 4.83, the traditional single-point optimized design, and the baseline airfoil.

Table II. Comparison of performances corresponding to robust optimized ($f_1 = 4.72$), traditional single-point optimized, and baseline airfoils.

	α	13°	14°	15°	16°	17°
Baseline airfoil	$\frac{C_l}{C_d}$	$\frac{4.2461}{0.1742}$	$\frac{4.3220}{0.1837}$	$\frac{4.3757}{0.1939}$	$\frac{4.4161}{0.2041}$	$\frac{4.4427}{0.2147}$
Optimized (Landing)	$\frac{C_l}{C_d}$	$\frac{4.6762}{0.2130}$	$\frac{4.7596}{0.2224}$	$\frac{4.8271}{0.2328}$	$\frac{4.8753}{0.2458}$	$\frac{4.9015}{0.2602}$
Robust optimized (Landing)	$\frac{C_l}{C_d}$	$\frac{4.7129}{0.2440}$	$\frac{4.7302}{0.2540}$	$\frac{4.7358}{0.2642}$	$\frac{4.7307}{0.2751}$	$\frac{4.7155}{0.2870}$

optimized design, but it can be higher for the rest of values of M_∞ producing a mean value better than the single-point case but with a bigger amount of sensitivity.

In conclusion, the Pareto front shown in Figure 7 allows to select designs with a small sensitivity than in the single-point one, but also with a smaller mean value of C_l, but we also obtain designs with a bigger mean value of C_l but with also a bigger sensitivity than in the single-point case.

7. CONCLUSION

The problem of aerodynamic shape optimization with uncertain operating conditions is addressed in this paper. It is solved by using the Taguchi concept converting design with uncertainties into a two-objective optimization problem: one objective is the mean performance, the other one is the variance of the performance. To overcome the difficulty related to the high computational cost required by robust design and GAs, a response surface modeling strategy is proposed that relies on the polynomial approximation, to estimate the fitness value. In addition, a semi-torsional spring analogy is used for the deformation of the computational mesh in order to fit it to the different geometries obtained during the shape optimization process.

This methodology is demonstrated for a realistic high-lift device's lift maximization in subsonic flow with fluctuation on free stream incidence angle. This optimization problem is solved using the proposed Taguchi robust control method successfully.

REFERENCES

1. Egorov IN, Kretinin GV, Leshchenko IA. How to execute robust design. *AIAA Paper No. 2002-5670*, *9th AIAA/USAF/NASA/ISSMO Symposium on Multidisciplinary Analysis and Optimization*, Atlanta, Georgia, 4–6 September 2002.
2. Chung H, Alonso J. Multiobjective optimization using approximation model based genetic algorithms. *AIAA Paper No. 2004-4325*, *Tenth AIAA/ISSMO Multidisciplinary Analysis and Optimization Conference*, Albany, NY, 30 August–1 September 2004.
3. Ferguson TS. *Mathematical Statistics*: *A Decision Theoretic Approach*. Academic Press: New York, 1967.
4. Welch WJ, Yu TK, Kang SM, Sacks J. Computer experiments for quality control by parameter design. *Journal of Quality Technology* 1990; **22**:15–22.
5. Roy RK. *A Primer on the Taguchi Method*. Competitive Manufacturing, Van Nostrand Reinhold: New York, 1990.
6. Huyse L. Free-form airfoil shape optimization under uncertainty using maximum expected value and second order second-moment strategies. *NASA/CR-2001-211020 or ICASE Report No. 2001-18*, 2001.
7. Deb K, Pratap A, Agarwal S *et al.* A fast and elitist multiobjective genetic algorithm: NSGA-II. *IEEE Transactions on Evolutionary Computation* 2002; **6**(2):182–197.

8. Schaffer JD. Some experiments in machine learning using vector evaluated genetic algorithms. TCGA file no. 00314. *Ph.D. Thesis*, Vanderbilt University, Nashville, TN, 1984.
9. Srinivas N, Dep K. Multiobjective optimization using nondominated sorting in genetic algorithms. *Evolutionary Computing* 1995; **3**:221–248.
10. Mäkinen RA, Toivanen J, Périaux J. Multidisciplinary shape optimization in aerodynamics and electromagnetics using genetic algorithms. *International Journal for Numerical Methods in Fluids* 1999; **30**(2):149–159.
11. Zitzler E, Thiele L. Multiobjective evolutionary algorithms: a comparative case study and the strength pareto approach. *IEEE Transactions on Evolutionary Computation* 1999; **3**:257–271.
12. Michalewicz Z. *Genetic Algorithms + Data Structures = Evolution Programs*. Springer: Berlin, 1992.
13. Deb K, Mohan M, Mishra S. Evaluating the epsilon-domination based multi-objective evolutionary algorithm for a quick computation of pareto-optimal solutions. *Evolutionary Computation* 2005; **13**(4):501–525.
14. Schutze O, Laumanns M, Coello CAC *et al.* Convergence of stochastic search algorithms to finite size pareto set approximations. *Journal of Global Optimization* 2008; **41**:559–577.
15. Giunta AA, Narducci R, Burgee S, Grossman B, Mason WH, Watson LT, Haftka RT. Variable-complexity response surface aerodynamic design of an HSCT wing. *AIAA Paper 95-1886, Proceedings of the 13th AIAA Applied Aerodynamics Conference*, San Diego, CA, June 1995; 994–1002.
16. Zeng D, Ethiera CR. A semi-torsional spring analogy model for updating unstructured meshes in 3D moving domains. *Finite Elements in Analysis and Design* 2005; **41**:1118–1139.
17. Blom FJ. Considerations on the spring analogy. *International Journal for Numerical Methods in Fluids* 2000; **32**:647.
18. Blom FJ, Leyland P. Analysis of fluid–structure interaction by means of dynamic unstructured meshes. *Journal of Fluid Engineering—Transactions of the ASME* 1998; **120**:792.
19. Chiandussi G, Bugeda G, Oñate E. A simple method for automatic update of finite element meshes. *Communications in Numerical Methods in Engineering* 2000; **16**:1–19.
20. Non-deterministic simulation for CFD-based design methodologies (NODESIM). *Project Supported by the European Commission Through the 6th Framework Programme as a Specific Targeted Research Project*. Available from: http://www.nodesim.eu/.
21. Deb K, Mohan M, Mishra S. Evaluating the epsilon-domination based multi-objective evolutionary algorithm for a quick computation of pareto-optimal solutions. *Evolutionary Computation* 2005; **13**:501–525.
22. Deb K, Pratap A, Agarwal S *et al.* A fast and elitist multiobjective genetic algorithm: NSGA-II. *IEEE Transactions on Evolutionary Computation* 2002; **6**:182–197.